Implementation of a microscopic nuclear potential in the coupled-channels calculations to study the fusion dynamics of oxygen-based reactions

N. Jain,[1,*] M. Bhuyan [2,†] and Raj Kumar [1,‡]

[1]*Department of Physics and Materials Science, Thapar Institute of Engineering and Technology, Patiala 147004, India*
[2]*Center for Theoretical and Computational Physics, Department of Physics, Faculty of Science,*
Universiti Malaya, Kuala Lumpur 50603, Malaysia

We incorporate a microscopic relativistic nuclear potential obtained from the recently developed relativistic R3Y NN potential in the coupled-channels code CCFULL to study fusion dynamics. The R3Y NN potential and the densities of interacting nuclei are obtained for the relativistic mean-field approach for the NL3* parameter set. Note that the R3Y NN potential can be expressed in terms of masses of the mesons and their couplings by considering the meson degrees of freedom within the relativistic mean field, which has a form similar to the widely used M3Y potential. We focused on the fusion cross sections for *oxygen*-based reactions with targets from different mass regions of the periodic table, i.e., $^{16}O + {}^{24}Mg$, $^{18}O + {}^{24}Mg$, $^{16}O + {}^{148}Sm$, $^{16}O + {}^{176}Hf$, $^{16}O + {}^{176}Yb$, $^{16}O + {}^{182}W$, and $^{16}O + {}^{186}W$. A comparison is also made with the cross sections calculated using the nuclear potential obtained from the traditional Woods-Saxon potential and the widely used M3Y NN potential within CCFULL. The coupled-channels calculations are performed with shape and rotational degrees of freedom to examine the fusion enhancement at below-barrier energies. It is observed from the calculations that the fusion cross sections obtained using the R3Y NN potential with rotational degrees of freedom are found to be more consistent with the experimental data than those for the M3Y and Woods-Saxon potentials, mainly at below barrier energies.

DOI: 10.1103/PhysRevC.109.034617

I. INTRODUCTION

The fusion reactions of heavy nuclei have been thoroughly studied to comprehend the quantum tunneling phenomenon in detailed studies of many-body systems [1–4]. Analyzing data from fusion reactions gives ample insight into synthesizing new elements or superheavy nuclei to extend the periodic table. The one-dimensional (1D) barrier penetration model (BPM) is used to compute the fusion cross section in the most basic description of nuclear fusion reactions [5]. The single fusion barrier can be viewed as breaking into the distribution of barriers. However, the coupling effects resulting from the vibrational, rotational, and neutron transfer degrees of freedom [2,6–11] must be considered when the collision energy is in the sub-barrier energy regime. The description of the fusion cross sections has been done with the help of several coupled-channels (CC) codes [12–15], of which the CCFULL code is frequently employed in fusion reaction cross-section calculations [16–18]. Furthermore, the study of fusion characteristics at extreme sub-barrier energies is crucial for understanding the reaction mechanisms in astrophysics and synthesizing superheavy nuclei [2,19,20]. While nuclear structure effects dominate below the Coulomb barrier, the

centrifugal potential suppresses these effects near or above the barrier. Nevertheless, the nuclear interaction component still needs to be understood [21–24]. The study of fusion dynamics is crucially dependent on understanding the pivotal role played by the nuclear potential. Interestingly, the nuclear potential determines both the shape of the potential and the height of the Coulomb barrier as prescribed by the well-known Wong formula [25]. Furthermore, the nuclear potential of the ground state affects the nuclear coupling to the excitation states of the colliding nuclei. Consequently, several nuclear potentials have been used in the coupled-channels approach to explain the fusion of heavy ions using the 1D BPM [26–28].

Various theoretical approaches have been developed to obtain and explain the nuclear potential between two colliding nuclei. One well-known method is the double-folding approach, where the ion-ion optical potential is derived by integrating an effective NN interaction and nuclear densities. This approach has been successfully applied to study nuclear clusters, proton-radioactivity, fusion, and elastic and inelastic scattering [29–34]. The nuclear densities, obtained using the Woods-Saxon ansatz, two-parameter Fermi (2pF), three-parameter Fermi (3pF), and Skyrme Hartree-Fock (SHF) models and the M3Y effective NN potential, are used to calculate the nuclear potential within the double-folding approach; see [35,36], among other works. The nonrelativistic M3Y NN potential is expressed as the sum of one-pion exchange potential (OPEP) and Yukawa terms, fitted to reproduce the

---

*nishujain1003@gmail.com

†bunuphy@um.edu.my

‡rajkumar@thapar.edu

G-matrix elements on an oscillator basis. In essence, the two crucial inputs in the double-folding approach are the densities of interacting nuclei and the *NN* potential (M3Y), obtained from two independent approaches. On the other hand, the nuclear potential for the interacting nuclei is generated via the Woods-Saxon (WS) potential in the CCFULL code [14], a simple empirical formula fitted for the known region of the nuclear chart. The Woods-Saxon potential, composed of depth, range, and diffuseness parameters, is widely used for approximating the shape of the nuclear component of nucleus-nucleus interactions [37,38]. The parameters of the WS potential are chosen to fit the experimental fusion cross section, mainly at above-barrier energies. However, the synthesis of exotic nuclei far from the β-stable region of the nuclear chart requires the adoption of a microscopic nuclear potential to study the fusion dynamics of the exotic region of the nuclear chart, as discussed in our previous work [39] and references therein.

At the microscopic level, the Skyrme-Hartree-Fock (SHF) and the relativistic mean-field (RMF) model [40] can be used to construct a nuclear interaction potential from a double-folding procedure. At low energy, nucleon-nucleon interactions are instantaneous, allowing for the concept of an interaction potential via an intermediate particle. The resulting nucleon-nucleon (NN) interaction potential, derived through particle exchange, is a significant tool for the understanding of nuclear forces and structure properties [41,42]. A double-folding procedure is used to calculate an optical potential between two interacting nuclei using this fundamental *NN* interaction [43–45]. Recently, the relativistic R3Y effective *NN* potential has been used in terms of meson masses and coupling constants and derived from the self-consistent relativistic mean-field (RMF) approach for a particular parameter set. Further, the densities are also calculated for the same parameter sets for both interacting nuclei, which are simultaneously used in the double-folding model. This enables the advancement of the theoretical approach to obtain the nuclear potential through meson interaction and also keeps the consistency of the parametrization for the *NN* potential and densities. It is to be noted that RMF models have proved to be highly predictive in the structural features of finite nuclei for β-stable and also highly isospin asymmetric regions of the nuclear chart [29,33,34,43,44,46–51].

Furthermore, applying the relativistic *NN*-interaction potential along with nuclear densities from the RMF formalism has proved successful in describing various nuclear phenomena such as clustering, proton radioactivity, and nuclear fusion [43–45]. Combining the relativistic R3Y potential with the RMF density is a compelling approach for investigating low-energy fusion reactions across various systems. In our previous works, the M3Y and R3Y nucleon-nucleon potentials were used to explore fusion hindrance phenomena in selected Ni-based reactions and to calculate cross sections for synthesizing heavy and superheavy nuclei. Specifically, the fusion and/or capture cross sections calculated using the M3Y *NN* potential were compared to the relativistic R3Y *NN* potential for the NL3* parameter set in earlier studies. A similar approach was employed using the ℓ-summed Wong formula in our previous work; see [33,34,52] and references therein. These studies concluded that the relativistic R3Y potential

provides better agreement with experimental data than the M3Y potential [33,34,43,44,53,54]. The novelty of the present work lies in obtaining the nucleus-nucleus potential from a double-folding model using a relativistic potential that has not been used as input for coupled-channels calculations. Furthermore, incorporating proper structural effects within the microscopic approach using RMF cannot be underestimated or undervalued, as it plays a vital role in reaction studies. Therefore, the involvement of rotational degrees of freedom with the microscopic R3Y *NN* interaction potential is considered for the target nuclei, but is limited to spherical symmetry in our previous work [33,34,53]. Hence, the present study represents a significant step forward in developing the nuclear potential obtained using the RMF formalism and its application within the coupled-channels approach for studying fusion dynamics. The study includes reactions covering different mass regions, i.e., $^{16}\text{O} + {}^{24}\text{Mg}$, $^{18}\text{O} + {}^{24}\text{Mg}$, $^{16}\text{O} + {}^{148}\text{Sm}$, $^{16}\text{O} + {}^{176}\text{Hf}$, $^{16}\text{O} + {}^{176}\text{Yb}$, $^{16}\text{O} + {}^{182}\text{W}$, and $^{16}\text{O} + {}^{186}\text{W}$. The fusion cross sections for these reactions are analyzed at subbarrier energies using the M3Y and microscopic R3Y *NN* potentials for the NL3* parameter set, and further compared with the case of the static Woods-Saxon potential. A possible comparison will be made between the theoretical results and the experimental data [9,55–58] for the considered reaction systems. Thus, implementing the microscopic nuclear potential in the CCFULL code to study fusion dynamics becomes crucial and intriguing.

This paper is organized as follows: Section II gives an overview of the theoretical formalism used for calculations. Section III shows the findings of the coupled-channels calculations. The results and discussions of the current work are summarized in Sec. IV.

II. THEORETICAL FORMALISM

The coupled-channels approach (CCFULL) is employed in the present study, and offers a reasonable understanding of the nuclear fusion dynamics at energy near the barrier. Instead of focusing on single barrier penetration, this approach considers multidimensional barrier penetration. This method considers the influence of coupling between relative motion and intrinsic degrees of freedom of the interacting nuclei, mainly for calculating mean angular momenta and the fusion cross sections of the compound nucleus [2,11,14]. The standard approach for addressing the impacts of the coupling between relative motion and intrinsic degrees of freedom on fusion is to numerically solve the coupled-channels equations, which include all relevant channels [59,60]. The coupled-channels equations solved numerically within the CCFULL are given as

$$\left[\frac{-\hbar^2}{2\mu} \frac{d^2}{dr^2} + \frac{J(J+1)\hbar^2}{2\mu r^2} + \frac{Z_P Z_T e^2}{r} + V_N + \epsilon_n - E_{\text{c.m.}} \right]$$
$$\times \psi_n(r) + \sum_m V_{nm}(r)\psi_m(r) = 0. \tag{1}$$

Here r represents the radial part of relative motion between the colliding nuclei, and μ is known as the reduced mass of the interacting system. ϵ_n is the excitation energy for the nth channel and $E_{\text{c.m.}}$ is the bombarding energy in the

center of the mass frame. V_N is the nuclear potential, and V_{nm} represents the matrix elements of the coupled Hamiltonian. Since there are several coupled-channels equations, their dimension is also significant. To reduce the dimension of coupled-channels equations, rotating frame approximation or no-Coriolis approximation is used [11,14,61]. The CC equations with nonlinear coupling are significant in studying the heavy-ion fusion reactions mainly at sub-barrier energies. All these sets of nonlinear coupling are taken into account.

The boundary condition for the incoming wave [62] is also necessary for the solution of the coupled-channels equation as it is sensitive to the potential pocket of the interaction fusion barrier. The incoming wave of the entrance channel is at the minimum position ($r = r_{\min}$) of the barrier and the outgoing wave of other channels is at an infinite position. By involving the effect of the prominent intrinsic channels, the fusion cross sections are calculated as

$$\sum_J \sigma_J(E) = \sigma_{fus}(E) = \frac{\pi}{k_0^2} \sum_J (2J+1) P_J(E). \quad (2)$$

Here, the isocentrifugal approximation is used, and the total angular momentum J is substituted in place of ℓ for each channel by using the following equation:

$$\begin{aligned}
\langle \ell \rangle &= \sum_J J\sigma_J(E) \Big/ \sum_J \sigma_J(E) \\
&= \left(\frac{\pi}{k_0^2} \sum_J J(2J+1) P_J(E) \right) \Big/ \\
&\quad \left(\frac{\pi}{k_0^2} \sum_J (2J+1) P_J(E) \right),
\end{aligned} \quad (3)$$

where $P_J(E)$ is the total transmission coefficient. The crucial ingredient of the coupled-channels approach is the nucleus-nucleus interaction potential, which is taken as a Woods-Saxon form for the known region of the nuclear chart:

$$V_N = \frac{-V_0}{1 + \exp[(r_0 - R_0)/a_0]}, \quad (4)$$

where V_0, r_0, and a_0 are the nuclear potential parameters. In heavy-ion fusion reactions, the parameter of nuclear potential is on equal footing with that of nuclear structure degrees of freedom. Parallel to the traditional Woods-Saxon potential, here we employ the nuclear potential obtained from widely used M3Y [29] and relativistic R3Y [43–45] NN potentials for the NL3* parameter set. It is worth mentioning that the nuclear potential obtained from the relativistic mean field is for the first time introduced in the CCFULL for the study of fusion dynamics.

The recently developed R3Y NN potential can be obtained from the static solution of the field equations for mesons [33,43,45], and can be written as

$$\begin{aligned}
V_{\text{eff}}^{R3Y}(r) &= \frac{g_\omega^2}{4\pi} \frac{e^{-m_\omega r}}{r} + \frac{g_\rho^2}{4\pi} \frac{e^{-m_\rho r}}{r} - \frac{g_\sigma^2}{4\pi} \frac{e^{-m_\sigma r}}{r} \\
&\quad + \frac{g_2^2}{4\pi} r e^{-2m_\sigma r} + \frac{g_3^2}{4\pi} \frac{e^{-3m_\sigma r}}{r} + J_{00}(E)\delta(r), \quad (5)
\end{aligned}$$

Here, the parameters g_σ, g_ω, and g_ρ denote the respective coupling constants of the mesons having masses m_σ, m_ω, and m_ρ, respectively. g_2 and g_3 are the coupling constants of the nonlinear terms of the self-interacting σ field. J_{00} is the one-pion exchange potential (OPEP), and details can be found in Ref. [29]. Here we have used a revisited version of the widely used NL3 force [63], the so-called NL3* parameter set [64]. In the same pattern, the M3Y NN potential can be expressed as

$$V_{\text{eff}}^{\text{M3Y}}(r) = 7999 \frac{e^{-4r}}{4r} - 2134 \frac{e^{-2.5r}}{2.5r} + J_{00}(E)\delta(r). \quad (6)$$

Here, the range unit is in fm and the strength is in MeV. More details of Eqs. (5) and (6) can be found in Refs. [29,33,43,44,65]. The interaction potential between the projectile and target nuclei, considering their respective calculated nuclear densities ρ_p and ρ_t with the RMF approach for the NL3* parameter, can be determined using

$$V_n(\vec{R}) = \int \rho_p(\vec{r}_p)\rho_t(\vec{r}_t)V_{\text{eff}}(|\vec{r}_p - \vec{r}_t + \vec{R}| \equiv r)d^3 r_p d^3 r_t, \quad (7)$$

the double-folding procedure [29] with the M3Y and relativistic R3Y interaction potentials proposed in Refs. [33,43,44]. Additionally, single nucleon exchange effects can be included through a zero-range pseudopotential.

The total nuclear interaction potential between the projectile and target nuclei can be obtained by combining the Coulomb potential with the nuclear interaction potential $V_n(R)$ obtained from Eq. (7), which is the main ingredient in the coupled-channels approach (CCFULL). One can generate the nuclear coupling Hamiltonian by changing the target radius in the nuclear potential [1] to a dynamical operator,

$$R_0 \rightarrow R_0 + \hat{O} = R_0 + \beta_2 R_T Y_{20} + \beta_4 R_T Y_{40}, \quad (8)$$

where R_T is $r_{\text{coup}}A^{1/3}$ and β_2 and β_4 are the quadrupole and hexadecapole deformation parameters of the deformed target nucleus, respectively. Thus, the nuclear coupling Hamiltonian is given by

$$V_N(r, \hat{O}) = \frac{-V_0}{1 + \exp[(r_0 - R_0 - \hat{O})/a_0]}. \quad (9)$$

In order to connect the $|n\rangle = |I0\rangle$ and $|m\rangle = |I'0\rangle$ states of the target's ground rotational band, we need matrix elements of the coupling Hamiltonian. These are readily accessible using matrix algebra [66]. In this algebra, the eigenvalues and eigenvectors are of the operator $\hat{O}$, which satisfies

$$\hat{O}|\alpha\rangle = \lambda_\alpha |\alpha\rangle \quad (10)$$

This is implemented in the CCFULL program by diagonalizing the matrix $\hat{O}$, whose elements are given by

$$\begin{aligned}
\hat{O}_{II'} &= \sqrt{\frac{5(2I+1)(2I'+1)}{4\pi}} \beta_2 R_T \begin{pmatrix} I & 2 & I' \\ 0 & 0 & 0 \end{pmatrix}^2 \\
&\quad + \sqrt{\frac{9(2I+1)(2I'+1)}{4\pi}} \beta_4 R_T \begin{pmatrix} I & 4 & I' \\ 0 & 0 & 0 \end{pmatrix}^2. \quad (11)
\end{aligned}$$

The nuclear coupling matrix elements are then evaluated as

$$V_{nm}^{(N)} = \langle I0 \mid V_N(r, \hat{O}) \mid I'0 \rangle - V_N^{(0)}(r)\delta_{n,m},$$

$$= \sum_\alpha \langle I0 \mid \alpha \rangle \langle \alpha \mid I'0 \rangle V_N(r, \lambda_\alpha) - V_N^{(0)}(r)\delta_{n,m}. \quad (12)$$

The last term is included in the equation to avoid the diagonal componentbeing counted twice. The CCFULL program incorporates the Coulomb interaction of the deformed target up to the second order in β_2 and the first order in β_4. The higher-order couplings of the Coulomb interaction have a relatively minor impact, unlike the nuclear couplings. The matrix elements of the Coulomb interaction potential can be expressed as follows:

$$V_{R(I,I')}^C = \frac{3Z_P Z_T R_T^2}{5r^3} \sqrt{\frac{5(2I+1)(2I'+1)}{4\pi}}$$

$$\times \left(\beta_2 + \frac{2}{7}\beta_2^2\sqrt{\frac{5}{\pi}}\right)\begin{pmatrix} I & 2 & I' \\ 0 & 0 & 0 \end{pmatrix}^2$$

$$+ \frac{3Z_P Z_T R_T^4}{9r^5} \sqrt{\frac{9(2I+1)(2I'+1)}{4\pi}}$$

$$\times \left(\beta_4 + \frac{9}{7}\beta_2^2\right)\begin{pmatrix} I & 4 & I' \\ 0 & 0 & 0 \end{pmatrix}^2, \quad (13)$$

for rotational coupling. These coupled-channels equations are used to calculate the fusion cross-section of the compound nucleus by assuming the rotational degrees of freedom as discussed in Sec. III.

III. RESULTS AND DISCUSSIONS

The coupled-channels calculations adequately account for several degrees of freedom such as collective surface vibrations, rotations, and neutron transfer to reasonably explain the fusion crosssection with lower excitation energy. In the present study, the coupled-channels calculations with microscopic external potential are performed by using the following steps:

(1) The nucleus-nucleus potential is obtained from a double-folding model using the relativistic potential that has not been used as input to coupled-channels calculations, including low-lying rotational states of the deformed target nucleus among the channels.

(2) The structural bulk properties such as binding energy, nuclear radii, density distribution, and quadrupole (β_2) and hexadecapole (β_4) deformationsare obtained from relativistic mean field formalism, which gives a picture of the nuclei that are involved in the reaction.

(3) The density, and the shape's degrees of freedom, i.e., quadrupole (β_2) and hexadecapole (β_4), are incorporated through the nuclear potential to calculate the fusion cross section within the coupled-channels calculations.

(4) The rotational degrees of freedom up to 4^+ states are considered to examine the fusion enhancement at below-barrier energies.

TABLE I. The Woods-Saxon (WS) parameters (V_0, r_0, and a_0) and quadrupole (β_2) and hexadecapole (β_4) deformations calculated using RMF (with NL3* parameter set) are listed. The excitation energy corresponding to quadrupole deformation of the target nuclei is taken from Ref. [67].

	Woods-Saxon potential			Deformation target		
System	V_0 (MeV)	r_0 (fm)	a_0 (fm)	E_2^+ (MeV)	β_2	β_4
$^{16}O + ^{24}Mg$	45.93	1.17	0.61	1.368	0.416	0.004
$^{18}O + ^{24}Mg$	47.20	1.17	0.62	1.368	0.416	0.004
$^{16}O + ^{148}Sm$	62.20	1.17	0.65	0.550	0.112	0.049
$^{16}O + ^{176}Hf$	63.63	1.18	0.65	0.088	0.284	−0.041
$^{16}O + ^{176}Yb$	60.00	1.17	0.65	0.082	0.298	−0.057
$^{16}O + ^{182}W$	63.99	1.17	0.65	0.100	0.273	−0.056
$^{16}O + ^{186}W$	70.00	1.18	0.65	0.122	0.241	−0.094

It is worth mentioning that the primary reason for choosing the external nuclear potential obtained from RMF is that it provides valuable information on bulk nuclear properties such as binding energy, charge distributions, and single-particle energy levels. Further details on the applicability of the RMF model with various parametrizations can be found in Refs. [33,43,45] and references therein. In parallel, the Woods-Saxon (WS) potential within CC calculations is also used for comparison. The reactions $^{16}O + ^{24}Mg$, $^{18}O + ^{24}Mg$, $^{16}O + ^{148}Sm$, $^{16}O + ^{176}Hf$, $^{16}O + ^{176}Yb$, $^{16}O + ^{182}W$, and $^{16}O + ^{186}W$ are considered within the CCFULL code to estimate the fusion cross sections. Rotational degrees of freedom were considered for the target nuclei [9,55–58], while ^{16}O and ^{18}O are treated as spherical in the present analysis. The Woods-Saxon (WS) parametrizations of the AkyüzWinther (AW) potential, the excitation energy corresponding to the first excitation state [67], and the values of the deformation parameters (calculated using RMF with the NL3* parameter set) are listed in Table I. The potential parameters of the WS potential are chosen in such a way as to fit the experimental data at above-barrier energies for 1D BPM. The fusion barrier characteristics i.e., barrier height and position, are obtained using the above-mentioned potentials, namely WS, M3Y, and R3Y NN potentials. The variation of total interaction potential, which is given by the sum of Coulomb and nuclear potential, at $\ell = 0\hbar$ with the separation distance r, is shown in Fig. 1 and inset of Fig. 3 for the considered choice of reactions. The solid black and dotted blue line represents the interaction potential corresponding to WS and R3Y NN potentials while the dashed red line represents the M3Y NN potential. It can be observed from these figures that the barrier formed in the case of the M3Y NN potential and the WS potential is relatively higher in comparison to the relativistic R3Y NN potential (as discussed in our previous work [39]) for all the considered reactions. The results obtained from the above analysis suggest that the R3Y effective NN potential, formulated in terms of meson masses and coupling constants, generates a more attractive interaction potential than the M3Y NN and WS potentials. The fusion cross section of reaction systems is significantly influenced by the properties of the fusion barrier, highlighting the direct impact of barrier characteristics on the
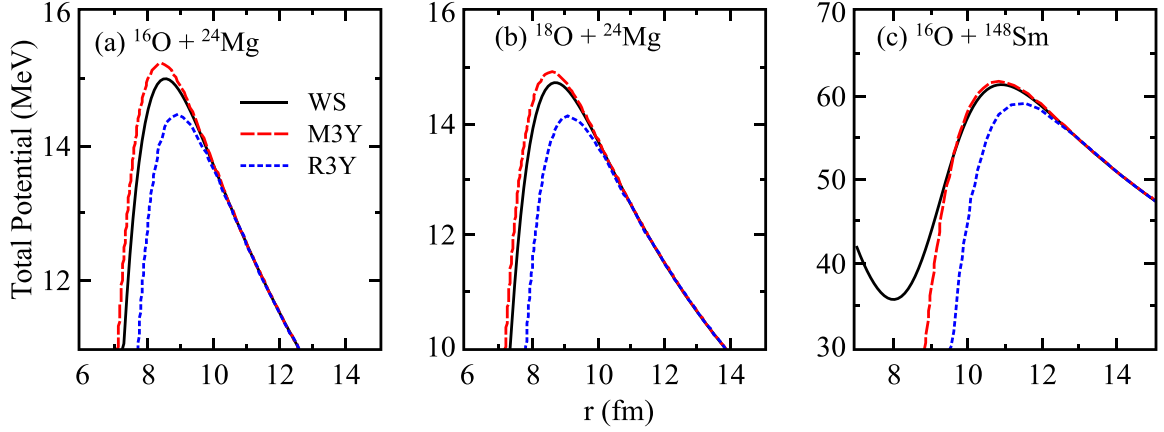
FIG. 1. The total interaction potential as a function of radial separation r for $^{16}O + ^{24}Mg$, $^{18}O + ^{24}Mg$, and $^{16}O + ^{148}Sm$ reactions calculated using the M3Y (dashed red lines) and R3Y (dotted blue lines) NN potentials. The microscopic nuclear potential is further compared with the traditional WS (solid black line) potential. See the text for details.

overall reaction dynamics. The higher the barrier height, the lower will be the fusion cross section. The effect of the above-discussed potentials on the fusion cross section is studied further with the help of coupled-channels calculations.

Following Ref. [68], we obtain the ℓ_{max} values from the sharp cutoff model [69] by using experimental data at above-barrier energies wherever available, and extrapolated for below barrier energies. As we mentioned above, the main aim of our work is to use the microscopic nuclear potential in the CCFULL code obtained from the recently developed R3Y NN potential. The calculated results are further compared with the cross section obtained using traditional WS and M3Y NN potentials. The RMF with NL3* parameter set is used

to obtain the relativistic R3Y NN potential using the density of the projectiles and targets, which are the main ingredients for nuclear potential. It is worth mentioning that the self-consistent relativistic mean-field formalism is successfully applied in the fusion hindrance reaction phenomena in our recent works [33,34,53]. Furthermore, the RMF with NL3* force parameter could provide the relativistic flavor to the fusion characteristics analogously to nuclear structure studies. We have used the relativistic R3Y NN potential and densities from the RMF approach for NL3* in the CCFULL calculation. The coupled-channels calculations are performed with rotational degrees of freedom to examine the fusion enhancement using the microscopic nuclear potential at below-barrier
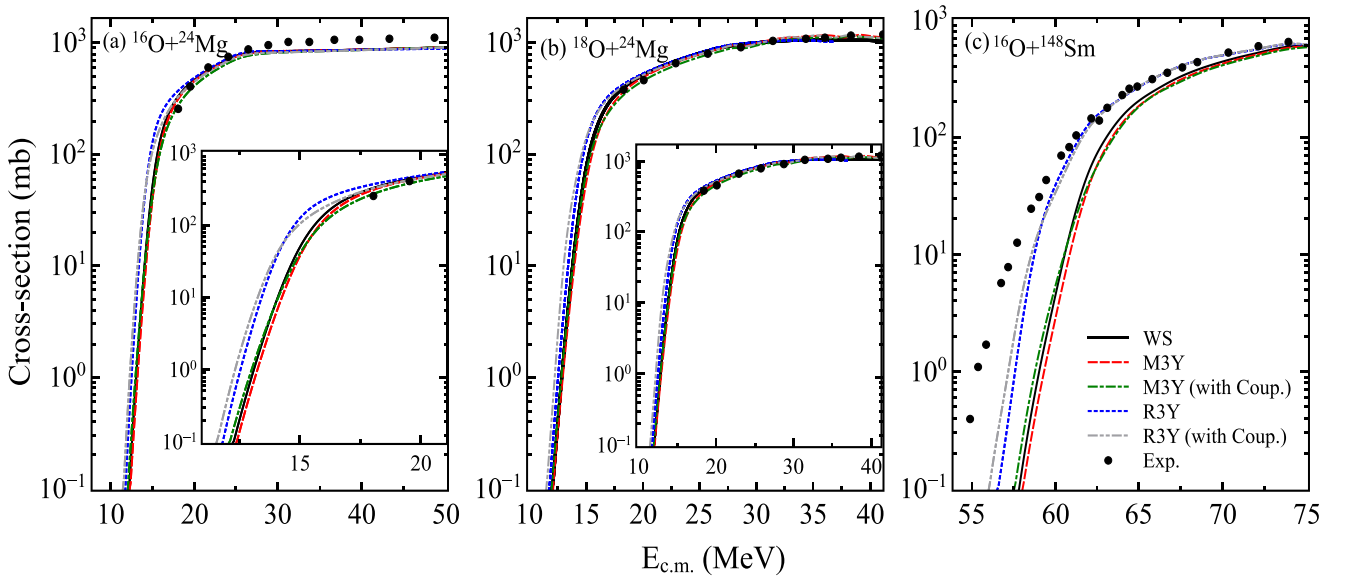

FIG. 2. The fusion cross sections as a function of $E_{c.m.}$ (MeV) for the Woods-Saxon potential (solid black line) and R3Y (dotted blue line) and M3Y (dashed red line) NN interactions with the NL3* parameter set using coupled-channels code. The corresponding cross section for the 4^+ excited state for R3Y (double-dotted–dashed grey line) and M3Y (dashed-dotted red line) potentials along with the inclusion of β_2 and β_4 deformations. The calculated results are compared with the experimental data [55,57] for $^{16}O + ^{24}Mg$, $^{18}O + ^{24}Mg$, and $^{16}O + ^{148}Sm$ reactions. See the text for details.
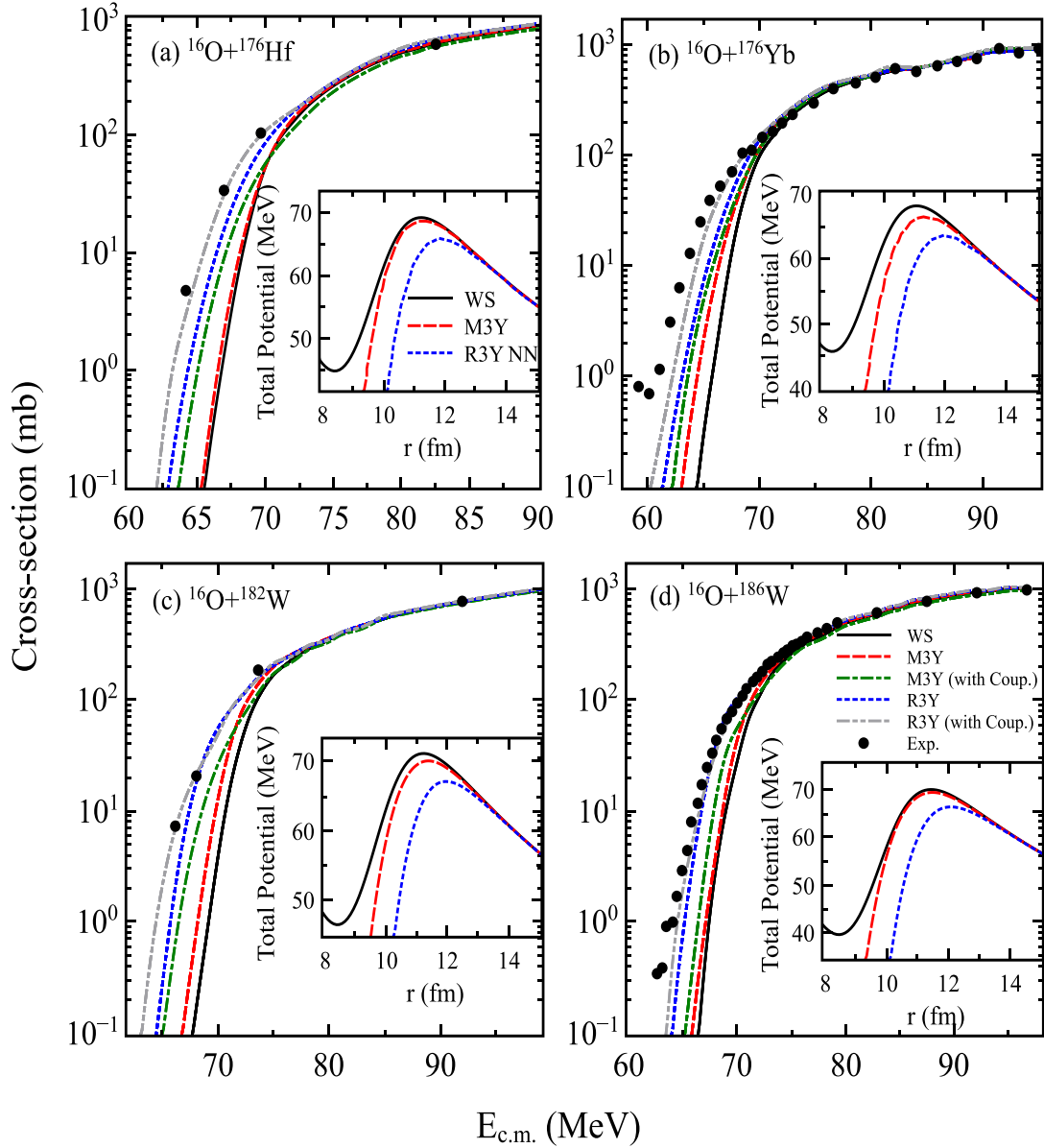
FIG. 3. Same as Fig. 2, but for $\beta_4 < 0$, namely reactions $^{16}\mathrm{O} + {}^{176}\mathrm{Hf}$, $^{16}\mathrm{O} + {}^{176}\mathrm{Yb}$, $^{16}\mathrm{O} + {}^{182}\mathrm{W}$, and $^{16}\mathrm{O} + {}^{186}\mathrm{W}$. The experimental data are taken from Refs. [9,56,58]. See the text for details.

energies. First we perform the one-dimensional barrier penetration model calculations by ignoring the nuclear intrinsic excitations to reproduce the experimental fusion cross sections at energies above the barrier [70]. The black (solid), red (dashed) and blue (dotted) lines represent the fusion cross sections obtained using WS, M3Y, and R3Y NN interaction potentials, respectively, for 1D BPM as shown in Figs. 2 and 3. The calculated fusion crosssections with 1D BPM underestimate the experimental data, particularly at below-barrier energies. Note that, in the present CCFULL calculations, only rotational degrees of freedom are considered to address the fusion cross section for the above-mentioned reactions. The two different conditions based on the shape (hexadecapole deformation) of nuclei, $\beta_4 > 0$ and $\beta_4 < 0$, are considered in the present work. Furthermore, it has been anticipated that the reactions involving nuclei either having positive or negative

hexadecapole deformation exhibit an increase in the fusion cross section at energies below the Coulomb barrier [71–76], which demands further experimental study.

The fusion cross sections calculated for $^{16}\mathrm{O} + {}^{24}\mathrm{Mg}$, $^{18}\mathrm{O} + {}^{24}\mathrm{Mg}$, and $^{16}\mathrm{O} + {}^{148}\mathrm{Sm}$ reactions having $\beta_4 > 0$ are shown in Fig. 2. To probe the possible generalizations concerning the behavior of the heavy-ion fusion process, first we discuss the fusion reaction of $^{16,18}\mathrm{O} + {}^{24}\mathrm{Mg}$. Another aspect of nuclear structure that inspired research of the $^{16,18}\mathrm{O} + {}^{24}\mathrm{Mg}$ reaction is the significant deformation and strong collectively of $^{24}\mathrm{Mg}$, which can potentially affect the fusion cross section. For example, the size of the nuclear surface density distribution, where low-energy heavy-ion reactions occur, and the deformation might enhance the fusion cross section. Furthermore, strong couplings to the collective degrees of freedom create a more efficient approach for kinetic energy transfer

to internal excitation and influence the fusion cross section. From Fig. 2(a), one can notice that the fusion cross section obtained for $^{16}O + ^{24}Mg$ reaction using the WS potential slightly deviates from the M3Y interaction potential cross section at near- and below-barrier energies. On the other hand, the fusion cross-section obtained with the WS potential overlaps with the R3Y NN potential cross section mainly at above-barrier energies. Furthermore, the fusion cross-section obtained using the R3Y NN interaction potential is comparatively larger than WS and M3Y interaction potentials mainly at below-barrier energies.

By including the excitation state of the target nuclei, the fusion cross section is enhanced particularly at below-barrier energies for M3Y (dotted-dashed green line) and R3Y (double-dotted–dashed grey line) NN interaction potentials and reasonably matches with the available experimental data [55]. This can be correlated with the weak magnitude of the β_4 value causing the enhancement observed in the case of M3Y and R3Y NN interaction potentials with the $(0^+ - 4^+)$ excitation state to be quite small compared to the 1D BPM. Similar results can be pointed out for $^{18}O + ^{24}Mg$ reaction. The cross section obtained using the WS potential overlaps with the M3Y and R3Y NN interaction potential cross sections at energies above the Coulomb barrier. More detailed inspections show a small increase in the fusion cross section for the R3Y NN interaction potential in comparison to the WS and M3Y interaction potentials and it is quite small for the $(0^+ - 4^+)$ excitation state as compared to the 1D BPM. Theoretical results obtained for these two reactions are consistent with the experimental data [55] over the available range of energies. More elaborately, the graph for the fusion cross section is plotted for $^{16}O + ^{24}Mg$ and $^{18}O + ^{24}Mg$ reactions in the narrower energy range in the inset of Figs. 2(a) and 2(b). The enhancement in the fusion cross section with the inclusion of a rotational excitation state is more clearly visible at energies below the Coulomb barrier. As shown in Fig. 2(c) for $^{16}O + ^{148}Sm$ reaction, the data obtained using WS and M3Y interaction potentials do not even fit the experimental cross section [57] data at the above-barrier energies. However the calculated results with the R3Y NN potential best match the experimental data near and above the Coulomb barrier energies. Also, the enhancement in the fusion cross sections with the inclusion of $(0^+ - 4^+)$ excitation channel can be observed with respect to the 1D BPM. It can be observed from the above-mentioned results with $\beta_4 > 0$ that the positive values of $\beta_4 > 0$ significantly affect the fusion cross section, and the results obtained using the R3Y NN potential with rotational excitation state are slightly superior to the M3Y and WS potentials for these considered systems. Further, with the inclusion of higher channels, a negligible effect on the fusion cross sections is observed.

A similar effect of the R3Y NN interaction nuclear potential can be observed for the reactions having negative values of the hexadecapole deformation of the target nuclei, $\beta_4 < 0$. The calculated fusion crosssection for all the considered systems, namely $^{16}O + ^{176}Hf$, $^{16}O + ^{176}Yb$, $^{16}O + ^{182}W$, and $^{16}O + ^{186}W$, having $\beta_4 < 0$ with WS, M3Y, and R3Y NN potentials (without coupling terms) gives the best match with the experimental data, especially at above-barrier energies.

However, fusion hindrance is still observed at energies below the Coulomb barrier. Therefore, the rotational excitation state of the target nuclei is included in the CC calculations. A detailed observation shows that the fusion cross-section obtained from M3Y potential exactly overlaps with the results obtained using the WS potential at energies below and above the Coulomb barrier for $^{16}O + ^{176}Hf$ as shown in Fig. 3(a). However, the fusion cross section obtained using the R3Y NN potential is more comparable to the M3Y and WS potential, mainly at sub-barrier energies. The fusion cross section obtained for the excitation state $(0^+ - 4^+)$ is higher than the 1D BPM for both M3Y and R3Y NN potentials below barrier energies. 1D data overestimated the excitation fusion cross-section for the M3Y potential at energies near and above the Coulomb barrier, which is related to the sharp cutoff model (choice of ℓ_{max} values). On the same footing, the results with the R3Y NN potential match well with the experimental data [56] even at below-barrier energies. Moreover, similar calculations were done for other reactions, namely $^{16}O + ^{176}Yb$, $^{16}O + ^{182}W$, and $^{16}O + ^{186}W$, as shown in Figs. 3(b), 3(c), and 3(d). The experimental data are given for comparison [9,56,58]. From the figures, one can observe that for $\beta_4 < 0$ the significant effect of the $(0^+ - 4^+)$ excitation state on the fusion cross section can be observed for R3Y NN potential as compared to the 1D BPM with M3Y and WS potentials. In other words, the fusion cross sections obtained with the inclusion of the $(0^+ - 4^+)$ excitation state in the R3Y NN potential are relatively closer to the experimental data at below- and above-barrier energies. As predicted above, we again observed that the fusion cross section obtained from the R3Y NN interaction potential with NL3* parameter set is found to be more consistent than those of WS and M3Y potentials mainly at below-barrier energies, except for the $^{16}O + ^{148}Sm$ reaction at energies below the Coulomb barrier. In contrast, the M3Y interaction only fits the data at above-barrier energies. Notably, the R3Y nuclear interaction explains the fusion cross section reasonably well at lower energies and consistently yields larger cross sections than the M3Y potential. Furthermore, we observe that with the inclusion of higher-order channels beyond 4^+ the higher-order channels cease to contribute significantly towards the fusion cross section around and below the Coulomb barrier. By the above analysis, it is evident from Figs. 2 and 3 that the recently established R3Y interaction for the NL3* force parameter with rotational degrees of freedom is a better choice than the WS and M3Y interaction potentials for the considered systems in fusion studies. Further, the implementation of the nuclear potential from RMF in the coupled-channels approach removes its dependency on the parameters of the Wood-Saxon potential, i.e., V_0, r_0, and a_0, as the potential here is obtained in a self-consistent way which makes the coupled-channels model more reliable. The Woods-Saxon parameters are otherwise tuned manually at the above-barrier energies for 1D BPM.

IV. SUMMARY AND CONCLUSIONS

In the present study, we have considered two different nucleon-nucleon interaction potentials: the widely used M3Y

potential and the relatively new relativistic R3Y interaction to estimate the fusion characteristics at low energies. The nuclear interaction potential is obtained for relativistic R3Y and M3Y NN potentials and corresponding interacting densities from the relativistic mean field approach for the NL3* parameter set by adopting the double-folding procedure. The coupled-channels CCFULL code is used to calculate the fusion cross section at below-barrier energies for these two kinds of nuclear potentials and to compare with the traditional Woods-Saxon (WS) potential. We considered seven reactions, namely $^{16}O + ^{24}Mg$, $^{18}O + ^{24}Mg$, $^{16}O + ^{148}Sm$, $^{16}O + ^{176}Hf$, $^{16}O + ^{176}Yb$, $^{16}O + ^{182}W$, and $^{16}O + ^{186}W$, in which target nuclei are rotational and ^{16}O, ^{18}O are considered as spherical in shape. In contrast to the expectation of 1D BPM, the sub-barrier fusion cross section is enhanced because of the coupling between the relative motion and the intrinsic degrees of freedom. The values of β_2 and β_4 deformation are calculated from the relativistic mean-field formalism for

the NL3* parameter set used in CCFULL to estimate the cross section. Interestingly, even a small change in the barrier height of the R3Y potential has a significant impact on the cross section, leading to a considerable increase in energies below the Coulomb barrier. From the fusion reactions at below-barrier energies, we observed that the R3Y interaction for the NL3* parameter set with rotational excitation state has proved to be a better option than the WS and M3Y potentials. As a result, it can be concluded that the R3Y interaction with NL3* causes interacting nuclei to recline, which lowers the barrier and raises the cross section at energies below the Coulomb barrier.

ACKNOWLEDGMENTS

[1] M. Dasgupta, D. J. Hinde, N. Rowley, and A. M. Stefanini, Annu. Rev. Nucl. Part. Sci. **48**, 401 (1998).

[2] A. B. Balantekin and N. Takigawa, Rev. Mod. Phys. **70**, 77 (1998).

[3] L. F. Canto, P. R. S. Gomes, R. Donangelo, and M. S. Hussein, Phys. Rep. **424**, 1 (2006).

[4] B. B. Back, H. Esbensen, C. L. Jiang, and K. E. Rehm, Rev. Mod. Phys. **86**, 317 (2014).

[5] N. Bohr and J. A. Wheeler, Phys. Rev. **56**, 426 (1939).

[6] M. S. Gautam, H. Khatri, and K. Vinod, Nucl. Phys. A **984**, 9 (2019).

[7] P. Jisha *et al.*, Phys. Rev. C **105**, 054614 (2022).

[8] T. Rajbongshi and K. Kalita, Cent. Eur. J. Phys. **12**, 433 (2014).

[9] T. Rajbongshi *et al.*, Phys. Rev. C **93**, 054622 (2016).

[10] H. Esbensen and S. Landowne, Phys. Rev. C **35**, 2090 (1987).

[11] K. Hagino and N. Takigawa, Prog. Theor. Phys. **128**, 1061 (2012).

[12] C. H. Dasso and S. Landowne, Comput. Phys. Commun. **46**, 187 (1987).

[13] J. Fernández-Niello, C. H. Dasso, and S. Landowne, Comput. Phys. Commun. **54**, 409 (1989).

[14] K. Hagino, N. Rowley, and A. T. Kruppa, Comput. Phys. Commun. **123**, 143 (1999).

[15] J. O. Newton, C. R. Morton, M. Dasgupta, J. R. Leigh, J. C. Mein, D. J. Hinde, H. Timmers, and K. Hagino, Phys. Rev. C **64**, 064608 (2001).

[16] K. Hagino, N. Takigawa, M. Dasgupta, D. J. Hinde, and J. R. Leigh, Phys. Rev. C **55**, 276 (1997).

[17] C. J. Lin, H. M. Jia, H. Q. Zhang, F. Yang, X. X. Xu, F. Jia, Z. H. Liu, and K. Hagino, Phys. Rev. C **79**, 064603 (2009).

[18] B. Mei, D. L. Balabanski, W. Hua *et al.*, Chin. Phys. C **45**, 054001 (2021).

[19] N. Rowley, G. R. Satchler, and P. H. Stelson, Phys. Lett. B **254**, 25 (1991).

[20] R. Vandenbosch, Annu. Rev. Nucl. Part. Sci. **42**, 447 (1992).

[21] R. Kumar, Phys. Rev. C **84**, 044613 (2011).

[22] D. Jain, R. Kumar, and M. K. Sharma, Nucl. Phys. A **915**, 106 (2013).

[23] R. Kumar, M. K. Sharma, and R. K. Gupta, Nucl. Phys. A **870-871**, 42 (2011).

[24] D. Jain, M. K. Sharma, Rajni, R. Kumar, and R. K. Gupta, Eur. Phys. J. A **50**, 155 (2014).

[25] C. Y. Wong, Phys. Rev. Lett. **31**, 766 (1973).

[26] H. J. Krappe, J. R. Nix, and A. J. Sierk, Phys. Rev. C **20**, 992 (1979).

[27] J. Blocki, J. Randrup, W. J. Światecki *et al.*, Ann. Phys. (NY) **105**, 427 (1977).

[28] R. Bass, Phys. Lett. B **47**, 139 (1973); Nucl. Phys. A **231**, 45 (1974).

[29] G. R. Satchler and W. G. Love, Phys. Rep. **55**, 183 (1979).

[30] G. Bertsch, J. Borysowicz, H. McManus, and W. G. Love, Nucl. Phys. A **284**, 399 (1977).

[31] D. T. Khoa, N. H. Phuc, D. T. Loan, and B. M. Loc, Phys. Rev. C **94**, 034612 (2016).

[32] Z. Gao-Long and L. Xiao-Yun, Chin. Phys. C **32**, 812 (2008).

[33] M. Bhuyan and R. Kumar, Phys. Rev. C **98**, 054610 (2018).

[34] M. Bhuyan, R. Kumar, S. Rana, D. Jain, S. K. Patra, and B. V. Carlson, Phys. Rev. C **101**, 044603 (2020).

[35] L. C. Chamon *et al.*, Phys. Rev. C **66**, 014610 (2002).

[36] http://nrv.jinr.ru/nrv/webnrv/elastic_scattering/Folding.pdf.

[37] L. Gan, Z.-H. Li, H.-B. Sun, S.-P. Hu, E.-T. Li, J. Zhong, Chin. Phys. C **45**, 054105 (2021).

[38] M. Gautam, Nucl. Phys. A **933**, 272 (2015).

[39] S. Rana, M. Bhuyan, and R. Kumar, Phys. Rev. C **105**, 054613 (2022).

[40] P. G. Reinhard, M. Bender, T. Buervenich, C. Reiss, J. Maruhn, and W. Greiner, Riken Rev. **26**, 23 (2000).

[41] S. Weinberg, Phys. Lett. B **251**, 288 (1990).

[42] D. B. Kaplan, M. J. Savage, and M. B. Wise, Nucl. Phys. B **534**, 329 (1998).

[43] B. B. Singh, M. Bhuyan, S. K. Patra, and R. K. Gupta, J. Phys. G: Nucl. Part. Phys. **39**, 025101 (2012).

[44] B. B. Sahu, S. K. Singh, M. Bhuyan, S. K. Biswal, and S. K. Patra, Phys. Rev. C **89**, 034614 (2014).

[45] M. Bhuyan, *Properties of Finite Nuclei using Effective Interaction: Structure of Drip-Line and Super-Heavy Nuclei in Effective*

Relativistic and Nonrelativistic Interactions (LAP Lambert Academic, Saarbrücken, Germany, 2014).

[46] P. Ring, Prog. Part. Nucl. Phys. **37**, 193 (1996).

[47] M. Bhuyan, B. V. Carlson, S. K. Patra, and S.-G. Zhou, Phys. Rev. C **97**, 024322 (2018).

[48] C. Lahiri, S. K. Biswal, and S. K. Patra, Int. J. Mod. Phys. E **25**, 1650015 (2016).

[49] B. D. Serot and J. D. Walecka, in *Advances in Nuclear Physics*, edited by J. W. Negele and E. Vogt (Plenum, New York, 1986), Vol. 16, p. 1.

[50] M. Bhuyan, Phys. Rev. C **92**, 034323 (2015).

[51] P.-G. Reinhard, Rep. Prog. Phys. **52**, 439 (1989).

[52] M. Bhuyan, S. Rana, N. Jain, R. Kumar, S. K. Patra, and B. V. Carlson, Phys. Rev. C **106**, 044602 (2022).

[53] S. Rana, R. Kumar, and M. Bhuyan, Phys. Rev. C **104**, 024619 (2021).

[54] J. T. Majekodunmi, M. Bhuyan, D. Jain, K. Anwar, N. Abdullah, and R. Kumar, Phys. Rev. C **105**, 044617 (2022).

[55] S. L. Tabor, D. F. Geesaman, W. Henning, D. G. Kovar, K. E. Rehm, and F. W. Prosser, Jr., Phys. Rev. C **17**, 2136 (1978).

[56] J. R. Leigh, J. J. M. Bokhorst, D. J. Hinde, and J. O. Newton, J. Phys. G **14**, L55 (1988).

[57] J. R. Leigh, M. Dasgupta, D. J. Hinde, J. C. Mein, C. R. Morton, R. C. Lemmon, J. P. Lestone, J. O. Newton, H. Timmers, J. X. Wei, and N. Rowley, Phys. Rev. C **52**, 3151 (1995).

[58] M. Trotta *et al.*, Eur. Phys. J. A **25**, 615 (2005).

[59] H. Esbensen, S. Landowne, and C. Price, Phys. Rev. C **36**, 1216 (1987).

[60] T. Rumin, K. Hagino, and N. Takigawa, Phys. Rev. C **61**, 014605 (1999).

[61] K. Hagino, S. Kuyucak, and N. Takigawa, Phys. Rev. C **57**, 1349 (1998).

[62] S. Landowne and S. C. Pieper, Phys. Rev. C **29**, 1352 (1984).

[63] G. A. Lalazissis, J. König, and P. Ring, Phys. Rev. C **55**, 540 (1997).

[64] G. A. Lalazissis, S. Karatzikos, R. Fossion, D. Pena Arteaga, A. V. Afanasjev, and P. Ring, Phys. Lett. B **671**, 36 (2009).

[65] L. I. Schiff, Phys. Rev. **84**, 1 (1951); **83**, 252 (1951).

[66] M. W. Kermode and N. Rowley, Phys. Rev. C **48**, 2326 (1993).

[67] S. Raman, C. W. Nestor, Jr., and P. Tikkanen, At. Data Nucl. Data Tables **78**, 1 (2001).

[68] R. Kumar, M. Bansal, S. K. Arun, and R. K. Gupta, Phys. Rev. C **80**, 034618 (2009).

[69] M. Beckerman, J. Ball, H. Enge, M. Salomaa, A. Sperduto, S. Gazes, A. DiRienzo, and J. D. Molitoris, Phys. Rev. C **23**, 1581 (1981).

[70] F. M. Zamrun, K. Hagino, and N. Takigawa, arXiv:nucl-th/0606011.

[71] N. Jain, M. Bhuyan, and R. Kumar, Phys. Scr. **98**, 025303 (2023).

[72] J. O. Fernández Niello, M. di Tada, A. O. Macchiavelli, A. J. Pacheco, D. Abriola, M. Elgue, A. Etchegoyen, M. C. Etchegoyen, S. Gil, and J. E. Testoni, Phys. Rev. C **43**, 2303 (1991).

[73] C. R. Morton, M. Dasgupta, D. J. Hinde, J. R. Leigh, R. C. Lemmon, J. P. Lestone, J. C. Mein, J. O. Newton, H. Timmers, N. Rowley, and A. T. Kruppa, Phys. Rev. Lett. **72**, 4074 (1994).

[74] M. J. Rhoades-Brown and V. E. Oberacker, Phys. Rev. Lett. **50**, 1435 (1983).

[75] R. C. Lemmon, J. R. Leigh, J. X. Wei, C. R. Morton, D. J. Hinde, J. O. Newton, J. C. Mein, M. Dasgupta, and N. Rowley, Phys. Lett. B **316**, 32 (1993).

[76] J. Fernández Niello and C. H. Dasso, Phys. Rev. C **39**, 2069 (1989).